6-2023

Liebau Pumping in Embryonic Hearts: A RIM-PIV Study of Liebau Impedance Pumping in an Embryonic Heart Model

Natalie Shearing
Union College - Schenectady, NY

Liebau Pumping in Embryonic Hearts: A RIM-PIV Study of Liebau Impedance Pumping in an Embryonic Heart Model

By

Natalie J. Shearing

* * * * * * * *

Submitted in partial fulfillment

of the requirements for

Honors in the Department of Mechanical Engineering

UNION COLLEGE

June 2023

Abstract

This work describes the design and implementation of a fully functioning, optically accessible Liebau pump with a visualization of the flow that will be generated using refractive index matched particle image velocimetry (RIM-PIV). Liebau impedance pumping is a unique way of transporting fluid by simply compressing a flexible tube; no valves are needed. The compression mechanism used in this design is a cam and follower mechanism, chosen for its ability to controllably pinch the tube, driving the flow.

In this work, RIM-PIV will be used to visualize the flow within the Liebau pump. To use this technique, the flexible tube of the pump was cast out of polydimethylsiloxane (PDMS) to match its refractive index to that of the glycerin water solution that the pump is submerged in and that is flowing within the pump. The resulting RIM-PIV measurements, which will be the first of their kind in a Liebau impedance pump, will contribute to the understanding of the velocity profile created within a Liebau pump and to answering the question of whether Liebau pumping is responsible for creating blood flow in the early stages of embryonic heart development.

Table of Contents

Table of Figures

Table of Tables

1 Introduction

1.1 Motivation

According to the American Heart Association, 13 in every 1,000 children in the U.S. are born with congenital heart defects each year [1]. However, the causes of these defects are still poorly understood. Gaining a better understanding of all aspects of embryonic heart development will be vital when it comes to determining where congenital heart defects come from and how they can be prevented.

One aspect of heart development that is not well understood is embryonic blood flow, despite it being well known that it plays an important role in heart development [2]. The pumping mechanisms responsible for the unidirectional blood flow in early-stage embryonic hearts are poorly understood and widely debated in the academic world. Early-stage embryonic hearts are little more than simple tubes, without any valves or other obvious mechanisms to create flow or control its direction. Some researchers have found evidence that peristaltic and Liebau pumping mechanisms could be possible drivers [3], while others have argued that their own simulations do not suggest either to be true [4-6].

A peristaltic pump is a positive displacement pump that works by compressing a tube in one location and then by sliding that pinch down the tube to push the fluid within it further along. Peristaltic pumping is already known to play a role in human biology (e.g. swallowing) and is believed to be a possible driver of embryonic blood flow. However, creating blood flow in the early-stage embryonic heart would require coordinated muscle activity that seems to be too complicated and coordinated for the simple, early-stage embryo.

On the other hand, Liebau pumping, being a simple, rhythmic compression in one location, seems to be simple enough for embryos at those early stages of development. Therefore, Liebau pumping is not only another possible blood flood driver, but maybe a more likely one. More research must be done to settle this debate and determine the real cause of embryonic blood flow.

1.2 Goal

The goal of this research is to design an optically accessible Liebau impedance pump. Then, to use RIM-PIV to analyze the flow generated by it. The resulting measurements, which will be the first of their type in a Liebau pump, will contribute to answering the question of whether Liebau pumping is responsible for creating blood flow in the early stages of embryonic heart development.

1.3 The Embryonic Heart

The fully developed human heart consists of valves and chambers that open, close, and contract to pump blood throughout the human body. However, in the early stages of embryonic development, these valves and chambers have not been formed yet. Instead, the embryonic heart begins as a simple straight, pulsating tube which somehow creates unidirectional blood flow. As development continues, the heart's geometry becomes progressively more complicated. For example, at its next stage in development, it goes through a c-looping stage that causes the tube to bend and twist as shown in Figure 1.1 below.

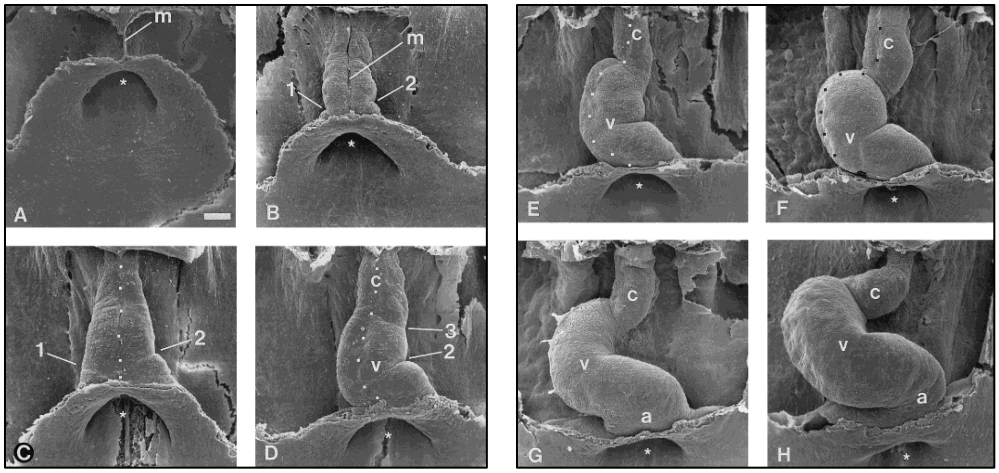

Figure 1.1. Cardiac c-looping at HH-stages 10, 11, and 12. Images A-C show the embryonic heart as a straight tube, while the images D-H step through the stages leading up to, including, and following the c-looping stage (HH-stage 12) [7].

In a simple particle tracking study, India ink was injected into a live chicken embryo to show blood flow in the aorta. By tracking the blood cells, the cardiac frequency was determined to be 2 Hz and the flow velocity was found to range from 0.12 to 3.2 mm/s. The blood flow was also confirmed to be pulsating, with measurably higher velocities immediately after each heartbeat, supporting the Liebau pumping theory [8].

Simulating the blood flow within the mechanism described in this report, and visualizing this proxy flow using RIM-PIV, will help determine if Liebau pumping is the source of this pulsating seen in actual embryonic hearts.

1.4 Liebau Pumping

Impedance is the natural resistance of a material to transferring a wave. It can be taken advantage of to create fluid flow. A Liebau impedance pump is a flexible tube that is filled with fluid and connected to something with a different impedance. The

flexible tube is pinched, displacing the fluid, and creating two traveling waves going in opposite directions away from the pinch site. Then, when the fluid reaches the impedance mismatch, at the boundary between the flexible tube and the rest of the system, a portion of the wave is reflected. Now, both waves are traveling in the same direction and the fluid between them is transported by the waves in that same direction. Therefore, simply by compressing a flexible tube in a noncentral location, unidirectional flow can be created. A visualization of this process can be seen in Figure 1.2 below.

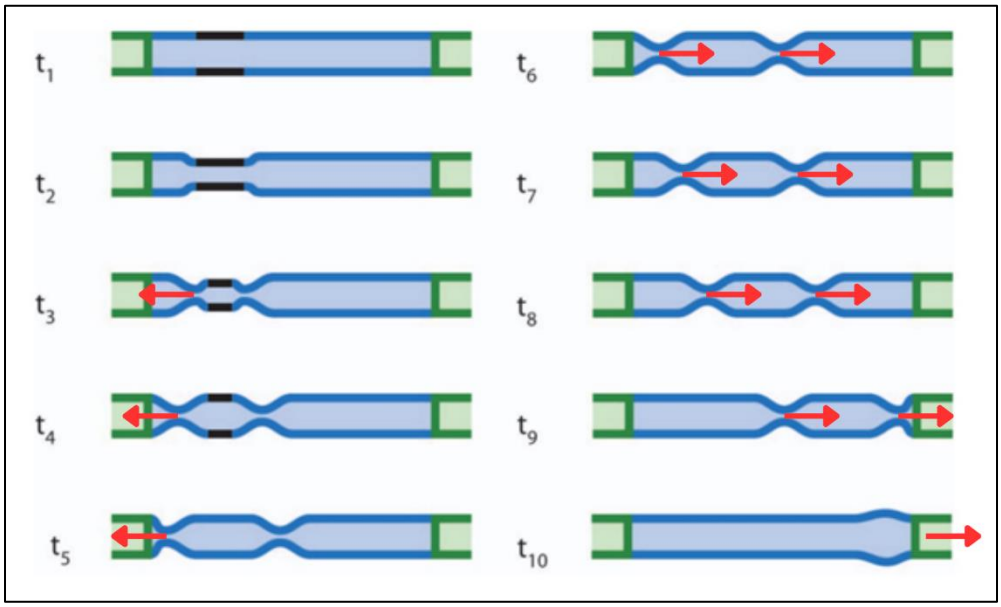

Figure 1.2. The blue section of the Liebau impedance pump is the flexible tube with its unique impedance, and the green sections have a different impedance. The flexible tube is compressed, displacing the fluid within the pincher, and creating waves. The waves reflect at the boundary between the unlike impedances causing the fluid to flow to the right [9].

Important parameters of a Liebau pump are the location, frequency, and amplitude of the compression, the elasticity of the tube, and the viscosity of the fluid. Changing these parameters will change the characteristics of the flow and some combinations will result in no net flow.

1.5 Literature Review

Since the discovery of the Liebau pump by Gerhart Liebau in 1954 [10], there have been many computational and analytical studies of impedance pumps [10]. However, there has been very little experimental investigation into the phenomenon. The little experimental work that has been done has been volumetric flow rate and pump head measurements [10]. There is a very large gap in the literature where flow visualization in a physical Liebau pump should be. Along with determining if Liebau pumping plays a role in embryonic blood flow, the goal of this research is to be the first to use RIM-PIV to visualize the internal flow in a Liebau pump.

1.6 Previous Work on the Project

This project is the design and implementation of a fully functioning, optically accessible Liebau pump with a visualization of the flow that will be generated using RIM-PIV. It is only a small portion of work done to answer a much larger question. The overall question being: How do embryonic hearts pump blood? To begin answering this, some researchers have investigated embryonic chicken hearts (which are comparable to human embryonic hearts in the early developmental stages) by particle tracing the blood flow [8], while others have hypothesized potential pumping mechanisms (Liebau, peristaltic, etc.), created models of those pumps, and tested them [3-6, 10]. However, the work done to make this project, the Liebau pump design, possible, began with casting a RIM tube [9].

1.6.1 Casting a Refractive Index Matched Flexible Tube

From there, the work to establish an in vitro model of Liebau pumping to be used to conduct flow visualizations was continued by Liam Nadire. He designed and constructed polydimethylsiloxane (PDMS) tubing. The tubing had to be flexible (cured to the correct hardness) and optically accessible (free from cloudiness, air bubbles, and scratches), which proved to be difficult to achieve. However, he was successful and could move on to developing a glycerin/water mixture that matched the index of refraction of the PDMS tubing. Nadire found that a PDMS tube with a solution of 55% glycerin and 45% water had an index of refraction mismatch of almost zero [9]. This work enables the use of RIM-PIV to visualize the flow within a Liebau pump, based on a flexible PDMS tube.

2 Design Problem Definition

2.1 Mimicking the Embryonic Heart

For the RIM-PIV flow visualization to contribute to determining if Liebau pumping plays a role in embryonic blood flow, the design of the embryonic heart model must mimic the embryonic heart as much as possible. First and foremost, the model must have a similar geometry to that of the embryonic heart. Therefore, it should have a straight, tubular geometry like that of the heart in the early stages of development. (Later on, to answer the bigger question that inspired this research, it might also be useful to have a model that is adaptable, allowing it to change tube shape, as the heart does when it bends and twists in the later looping stages of development.)

Beyond geometry, the model needs to be kinematically and dynamically similar to the actual embryonic heart. In other words, the flow patterns within the model have to match those in the real heart. Specifically, the velocities (kinematic) and forces (dynamic) acting at each point, in both the model and the actual heart, must scale to each other through the multiplication of a single constant. These two constants, one from the kinematic scaling and the other from the dynamic, become Pi groups that, through the Buckingham Pi Theorem, can be used to fully scale the model to the embryonic heart. Only with geometric similarity and kinematic and dynamic scaling will the results obtained from the model meaningfully reflect the situation occurring within the embryonic heart.

2.2 Compression Mechanism

To create a Liebau pump, a compression mechanism had to be designed. The mechanism had to compress the flexible tube at a variable location (along the axis of the flexible tube), with variable frequency and amplitude. These settings had to be precise and repeatable, meaning that they had to be lockable and clearly measurable and labeled, so they could be revisited easily.

The compression mechanism had to be designed with optical access in mind (Section 2.3). The design of the compression mechanism also had to account for the submergence of the heart model in a glycerin solution for RIM-PIV. This is because, to successfully achieve refractive index matching for RIM-PIV, the refractive indices of the PDMS tube (the tube being used to represent the embryonic heart tube) and the surrounding fluid (a glycerin-water solution) had to be the same.

(See Section 2.3 for reasoning behind using RIM-PIV.) With the flexible tube submerged, parts of the compression mechanism had to be waterproof. Additionally, the creation of waves on the free surface of the fluid had to be minimized.

2.3 Optical Access

In this experiment, RIM-PIV will be used to visualize the flow within a Liebau pump. To perform PIV, orthogonal laser, and camera access to the point of interest (the location of the compression) will be needed (Figure 2.1).

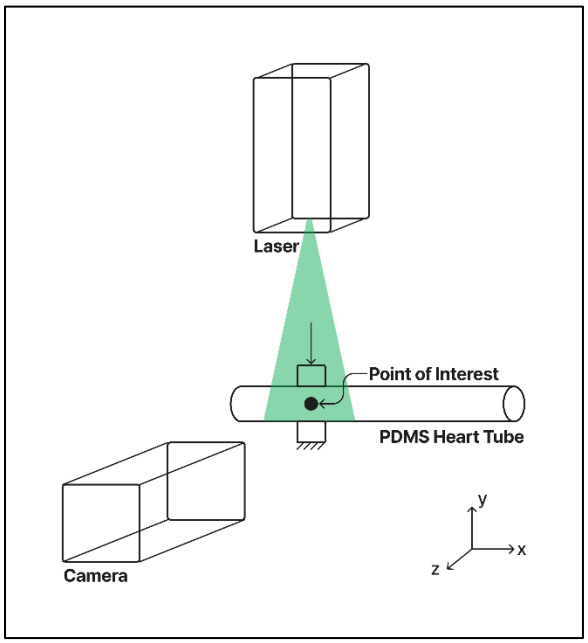

Figure 2.1. Optical layout including the camera along the z-axis, laser along the y-axis, and the PDMS model heart tube along the x-axis.

Ease of access for cleaning the PDMS tube interior walls and for air bubble releasing from the PDMS tube should also be taken into consideration when designing the setup. Cleaning will be necessary to remove any seeding build up on the interior walls of the PDMS tube, because clouded tube walls will reduce the

image quality. Releasing any air bubbles will be vital because they scatter the laser light, brightening the PIV images in undesired areas.

When using RIM-PIV, the refractive index of the fluid and the other components of the system are matched so light that passes through them is not bent. Essentially, when the system components are submerged and filled with the fluid, they disappear, because none of the light passing through them is being bent. Without refractive index matching, the light passing through the PDMS tube representing the embryonic heart will bend and distort the resulting PIV images. This bending can be reduced by using RIM-PIV. First, the flexible tube must have the same refractive index as the fluid surrounding it and flowing within it. This effect is demonstrated in Figure 2.2 below. Second, the parts of the system that must be immediately next to the flexible tube have to be operable in a liquid because they will be submerged in a liquid for the refractive index matching.

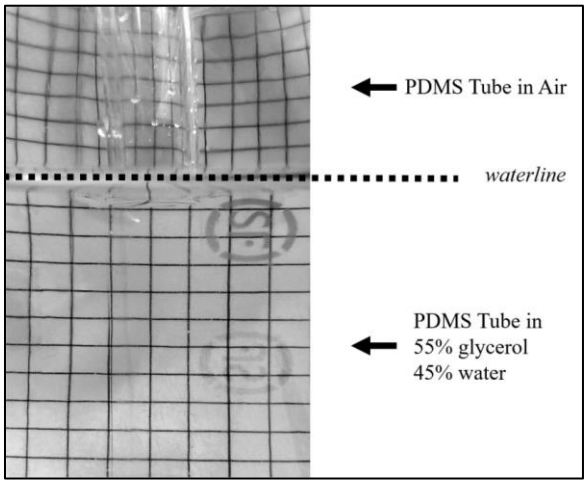

Figure 2.2. Refractive index matching where a PDMS tube is submerged in a 55% glycerin/45% water solution causing the tube to appear invisible [9].

Lastly, the entire setup is constrained to the size of the optics table in Union College's PIV lab. It can be no larger than 1.2 m x 2 m x 0.8 m.

3 Design Description

3.1 Compression Mechanism Design

The final design concept selected for the compression mechanism was a pivoting arm driven by an aluminum cam. A long pivoting arm was chosen to move most of the compression mechanism away from the heart tube to allow for better optical access. The aluminum arm is 30.5 cm long and contains a follower near the pivoting end and a long finger at the free end. A spring holds the arm up and presses the follower against the surface of the cam. The finger extends down, from the raised plate where the compression mechanism rests, to pinch the flexible tube against an anvil. The steel finger has a 25 mm diameter aluminum pinching attachment (Appendix B: Pincher #1) on its end to pinch the tube without cutting through it. The steel follower rises above the arm to the surface of the cam. It has a 10 mm outer diameter steel ball bearing that rolls along the cam profile. The cam profile is a cycloidal function that symmetrically rises and falls for $\pi/6$ radians each and dwells for $\pi/3$ radians. This function is repeated three times resulting in a three-lobed cam for three compressions every one rotation. All full description of the cam design can be found in Section 3.1.1 below. The cam is powered by a 313-rpm planetary gear motor. This motor was chosen, along with the three-lobed cam profile, to achieve a frequency of 2.5 compressions per second to create a Liebau pump, as estimated by performing hand compressions of the embryonic heart model. Together, the arm, cam, and motor pinch the flexible tube in a controlled, measurable manner.

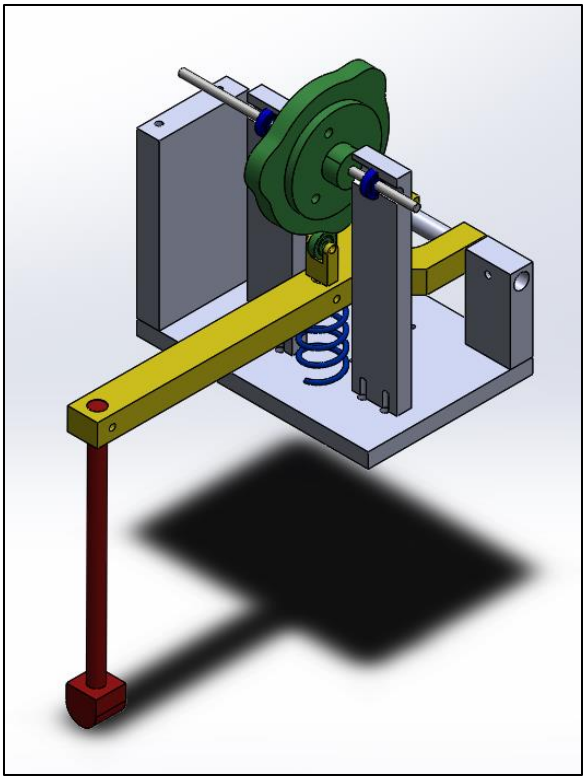

Figure 3.1. SOLIDWORKS model of compression mechanism design including pivoting arm (yellow), cam and roller follower (green), extension finger and pincher (red), and return spring (blue). The motor shaft rotates the cam and the arm pivots causing the pincher to compress the heart tube model (not shown).

A complete catalog of all parts purchased for this design can be found in the bill of materials (Appendix A). A complete set of detailed manufacturing drawings can be found in Appendix B.

3.1.1 Cam Design

A cam-and-follower mechanism was chosen to compress the tube because of its controllable amplitude and frequency. A cam profile is composed of rise, fall, and dwell sections. The rise section is when the radial distance of the cam's surface from its rotating axis is increasing, the fall section is when that distance is decreasing, and the dwell is when it remains the same (a circle of constant radius).

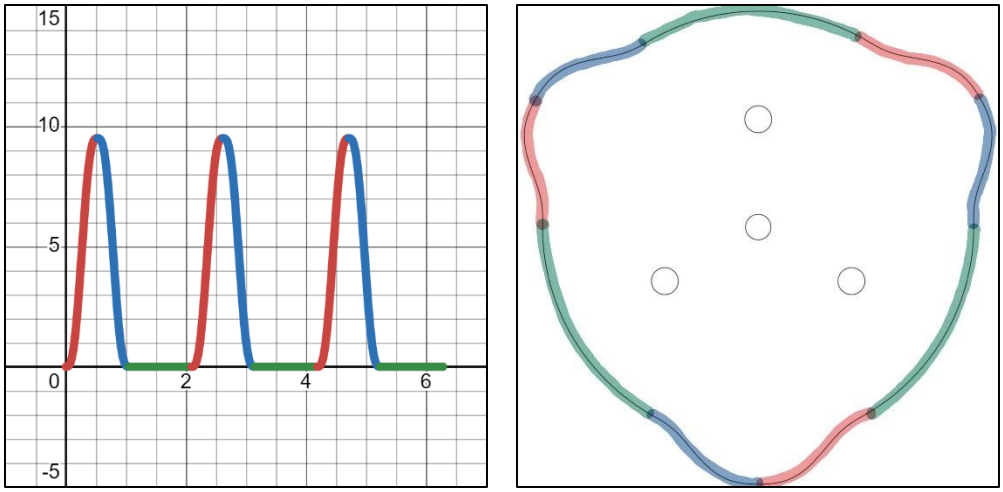

Figure 3.2. The cam profile function is graphed in the θ-y plane (left). In comparison, the physical cam profile is shown (right). The rise, fall, and dwell sections are shown in red, blue, and green, respectively.

The profile of the cam was chosen to be a cycloidal function to avoid discontinuities because it accelerates during the dwell of the function and has zero acceleration during the rise. This follower path is better because it reduces the amount of wear on the cam and follower as opposed to a simple harmonic, parabolic, or polynomial cam profile. The cycloidal function used to generate rise (Equation 3.1), fall (Equation 3.2), and dwell (Equation 3.3) sections of the cam profile are shown below.

$$s = h\left[\frac{\theta}{\beta} - \frac{1}{2\pi}\sin\left(2\pi\frac{\theta}{\beta}\right)\right] \tag{3.1}$$

$$s = 2h - h\left[\frac{\theta}{\beta} - \frac{1}{2\pi}\sin\left(2\pi\frac{\theta}{\beta}\right)\right] \tag{3.2}$$

$$s = 0 \tag{3.3}$$

In these equations, *s* represents the position of the follower as a radial distance from the rotating axis. The reference datum, where $s = 0$, is the dwell position of the follower, when the cam is not displacing the follower at all. In this case, that dwell

position is 50 mm from the rotating axis, meaning that if this cam had no rises or falls, the cam would be a circle with a radius of 50 mm. The h is the maximum displacement, in this case h = 9.5 mm. This value was determined by measuring the inner diameter of the PDMS tube (9.5 mm), because at maximum displacement, the tube should be fully compressed. The θ is the angle of the cam referenced to the starting position, ranging from 0 to 2π rad. The β is the period of each segment of the function (i.e., the period of each rise, fall, and dwell).

The period of each segment was chosen with trial and error. It was known from earlier experiments using hand compressions that a quick impulse with a long dwell in between pulses was the best way to produce Liebau pumping. Think karate chopping the tube: fast pinch, fast release, long break in between. To reproduce this using the cam, the profile had to have a fast rise and fall with long dwells in between. (This fast fall creates some problems described in later sections.) That said, they couldn't be too fast, or the torque required to drive the cam would be too much, and the cam and follower would lock up. Ultimately, after prototyping several options (Appendix C), the segment period was chosen to be $\beta = \pi/6$, resulting in a 3-lobed cam with each rise and fall lasting π/6 rad and each dwell lasting π/3 rad. (The dwell section is twice as long to replicate the long pause in between compressions that caused Liebau pumping using hand compressions.)

The cam profile function was programmed into MATLAB R2022b to output a matrix of xyz-coordinates (Appendix D). These coordinates were then saved and imported into SOLIDWORKS 2022 where a curve was generated and then extruded to create the cam (Appendix B). The cam was made of aluminum

because of availability, convenience, and machining-ease. The thickness was chosen to be 12.5 mm to be wide enough for the follower to remain on the surface of the cam and thin enough to cut the complex geometry using a water jet.

3.1.2 Follower Design

The follower of the cam had to be small enough to follow the cam profile precisely and durable enough to not wear. It also had to run smoothly enough to not wear the surface of the cam and have a friction low enough to not create too much torque on the cam and motor. A roller follower was chosen to help the follower run smoothly along the cam surface. The roller is made of a 5 mm inner diameter and 10 mm outer diameter ball bearing. Its width is 4 mm which fits well within the 12.5 mm width of the cam.

3.1.3 Arm Design

The major design constraints of the arm were weight and rigidness. The arm had to be lightweight, but rigid enough that it would not bend under the torque of the cam or the pinching pressure against the tube. The finger extending down from the arm also had to be rigid and light weight. The pincher attached to the finger had to be narrow enough to precisely locate the location of the compression and sufficiently rounded to avoid cutting or tearing the tube. The materials for these parts were chosen purely for convenience, both of material availability and manufacturing ease. The finger was made of a steel, 12.5 mm diameter, 305 mm long Thor Labs optics post that was already available in the lab and reused for this application.

3.1.4 Spring Sizing

The spring chosen for this system had a rate of 452 N/mm, an inner diameter of 12.5 mm, and an uncompressed length of 57 mm. This spring was specified by performing the following analysis. The arm, follower, finger, and pinching attachment were weighed to determine the required spring force. The total weight was measured to be F_s = 735 g. Using the total weight as the required spring force, assumes a static system. (A better assumption would be to include the inertial force of the arm in this calculation. See discussion, results, and recommendations for further details.) Preloading the spring, x = 12.5 mm was desired, so, using those values, Equation 3.4 below was used to determine the required spring rate.

$$F_s = kx \tag{3.4}$$

The required spring rate was calculated to be k = 362 N/mm. The free length of the spring was chosen to be a minimum of 50 mm because that is the distance between the cam-arm plate and the arm. (This assumption is wrong because it overlooks the previous desire to preload the spring 12.5 mm. The minimum length should have been 64 mm. See discussion, results, and recommendations for further details.) The final spring purchased had a free length of 55 mm. Additional springs of varying, but similar, lengths and rates were also purchased.

3.1.5 Motor Sizing

The motor used in this design is a planetary gear motor with a no-load speed of 313 rpm and a stall torque of 30 kg-cm. This motor was chosen based on availability and according to the following sizing analysis. These analyses were performed for

a previous prototype and the motor was grandfathered into the new design. It may not be, and probably isn't, the correct size for the new design. That said, the analysis described below can be used to find a new, properly sized motor.

The required motor torque was estimated to be T = 1.03 kg/cm using Equation 3.5 below.

$$T = 2kr\sin(\theta) \tag{3.5}$$

In this equation, T is the required motor torque, k is the spring rate, r is the radial distance from the axis of rotation to the maximum deflection point of the cam, and θ is the estimated angle at which the cam meets the follower. This is a quasi-static analysis that neglects inertial and frictional forces. However, the required torque was doubled to be conservative to ensure that the motor has more than enough power to rotate the cam.

The required motor speed, s = 150 rpm, was estimated by counting and timing hand compressions when creating flow within a Liebau pump by hand. The equation used to convert hand compressions to cam/motor revolutions is shown in Equation 3.6 below.

$$s = \frac{c}{l} \tag{3.6}$$

In this equation, s is the motor speed in rpm, c is the number of hand compression per minute, and l is the number of lobes on the cam.

The required motor power is the product of the required motor torque and speed. To pick a motor, compare the calculated required motor power and the maximum power of the potential motor and compare the calculated required motor

torque and the stall torque of the potential motor. The maximum power of the potential motor can be found using Equation 3.7 below.

$$P_{\max} = 0.25 T_{\text{stall}} s_{\text{NL}} \quad 3.7$$

In this equation, $P_{\max}$ is the maximum power, T_{stall} is the stall torque, and s_{NL} is the no load speed. When determining the correct motor, the required power should be less than the maximum power and the require torque should be less than half the stall torque.

To reiterate, for clarity, the numbers presented above, for both the required torque and the required motor speed, were based on a previous prototype. They do not apply to the design described in this report. However, the analysis still stands and can (and should) be used to find a motor to fit this design.

3.2 Heart Model Design

The final heart tube model is a straight, 3 mm thick PDMS tube with a 9.5 mm inner diameter. It is connected to two open reservoirs using plastic barbed fitting to NPT pipe connectors. A loop is created between the acrylic reservoirs by a second return tube that is located above and behind the PDMS tube. This Tygon tube has an inner diameter of 12.5 mm and is also connected with plastic barbed fitting to NPT pipe connectors. The width of the reservoirs and the diameter of the Tygon tube was chosen to be more than double the diameter of the PDMS tube to avoid creating too large of a head loss for the Liebau pump to overcome. The open reservoirs system was chosen for its easy access for seeding and cleaning as well as its ability to allow air bubbles to escape the system. In this design, the PDMS tube, representing the

early-stage straight heart tube, is compressed by the mechanism described above (Section 3.1). This creates a flow that pumps a glycerin solution through the PDMS tube, into one reservoir, back through the return tube, and into the other reservoir to be looped back through the PDMS tube once again.

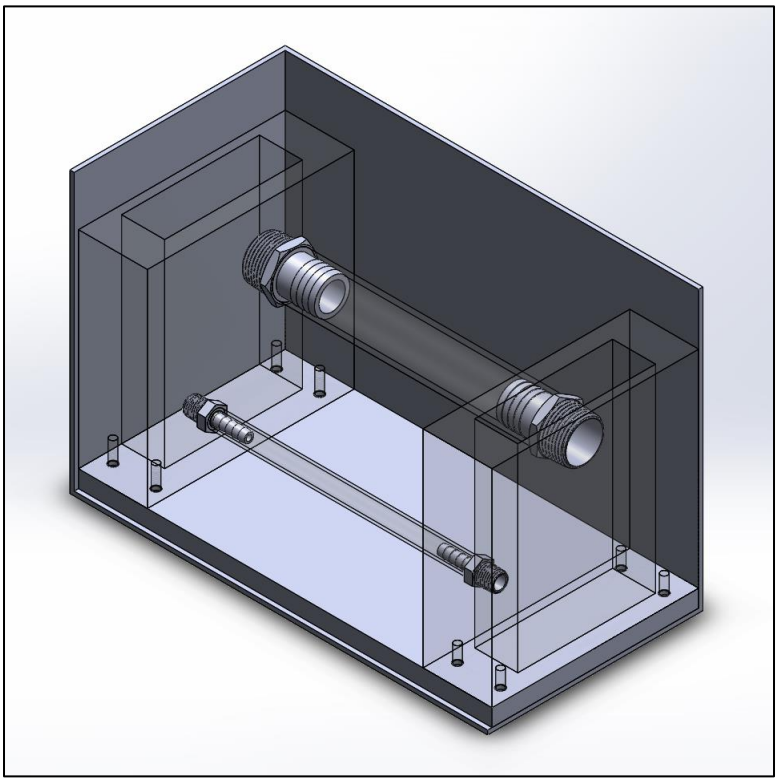

Figure 3.3. SOLIDWORKS assembly of heart model design including PDMS tube (lower tube), return tube (upper tube), reservoirs (left and right), and tank (surrounding).

3.2.1 Reservoir & Connecting Tube Design

The design for the reservoirs and connecting tube focused entirely on size. The reservoirs and tube had to large enough to avoid obstructing the flow created within the Liebau pump. Double the inner diameter (i.e., four times the available flow area) of the PDMS tube was assumed to be big enough. The entire system had to be small enough to fit into the tank to be fully submerged in the glycerin solution.

Beyond that, the internal volume of both the tank and the tube-reservoir system was designed to be as small as possible to save money and resources when filling them both with the glycerin solution and when seeding the tube-reservoir system. The material for the reservoir and the connection tube were chosen for cost and availability.

A detailed description of the PDMS tube design can be found in the undergraduate thesis of Liam Nadire, Union College ‘19 [9]. He designed and manufactured the tubes used in this design and in future experiments run with this Liebau pumping mechanism.

3.3 Optical Design

The entire heart model (both tubes and reservoirs) was submerged in a tank filled with a 55% glycerin/45% water solution. This was done to refractive index match the PDMS tube. The camera and laser are setup orthogonally with the camera facing perpendicular to the PDMS tube from the front and the laser pointing down on the PDMS tube from above. For now, images will be taken just to the side of the compression point until a hard, RIM material can be found to replace the aluminum pincher attachment. Hopefully, with this optical setup, RIM-PIV images can be taken of the flow created in the Liebau pump.

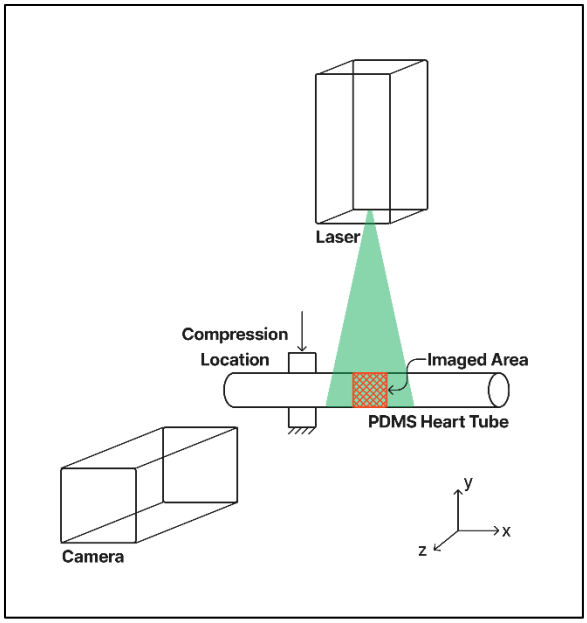

Figure 3.4. Optical design schematic showing the imaged area in relation to the compression location.

3.4 Adjustability

One of the most important design constraints was the adjustability of the compression location, frequency, and amplitude. All three of these variables have been incorporated into the design. The location of the compression along the PDMS tube can be adjusted using a linear optical mount stage. This location can be altered with 0.25 mm precision. The frequency of the compression can be altered in two ways. The first is by changing the motor speed. The second is by altering the cam profile to include a different number of lobes or to adjust the period of the rise and fall of the profile's cycloidal function. The amplitude of the compression can be changed by raising or lowering the scissor lift jack (shown in Figure 4.1) that the compression mechanism rests on. The jack has more than enough range to alter the amplitude from complete closure to none. With these variables included in the design, the correct combinations can be found to create a Liebau pump.

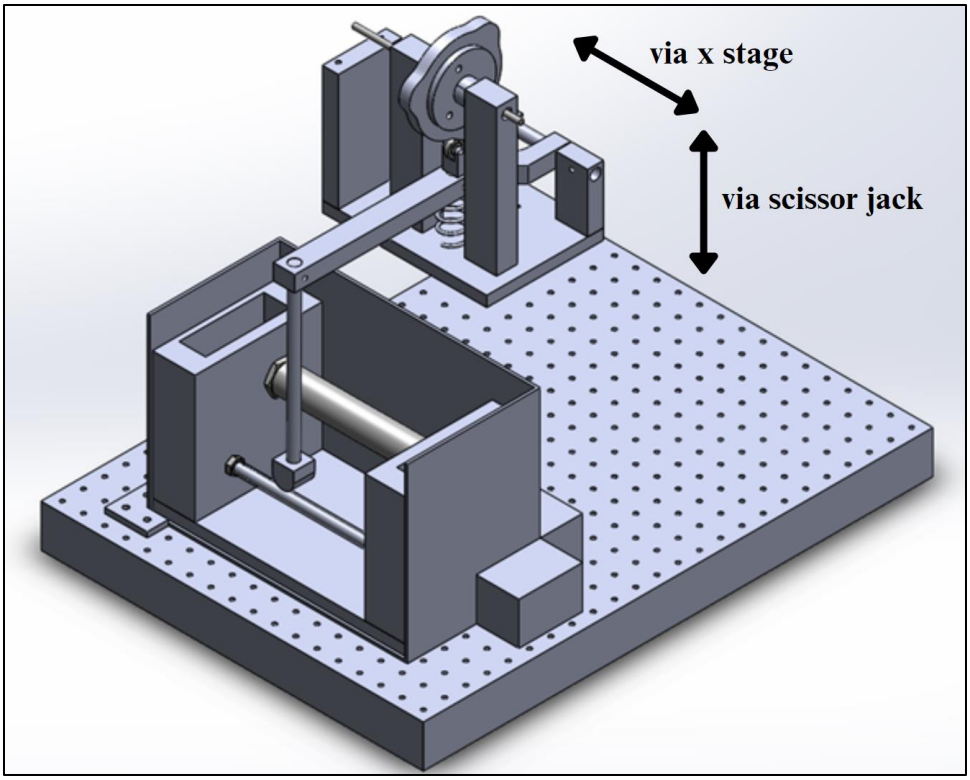

Figure 3.5. Final design including the compression mechanism and heart model designs.

4 Results

The final design described previously in the design description has been fully manufactured, assembled, and tested as shown in Figure 4.1 below. However, there are some issues that were revealed by testing that need to be addressed before visualization of the flow can begin. Therefore, there are no RIM-PIV test results to report.

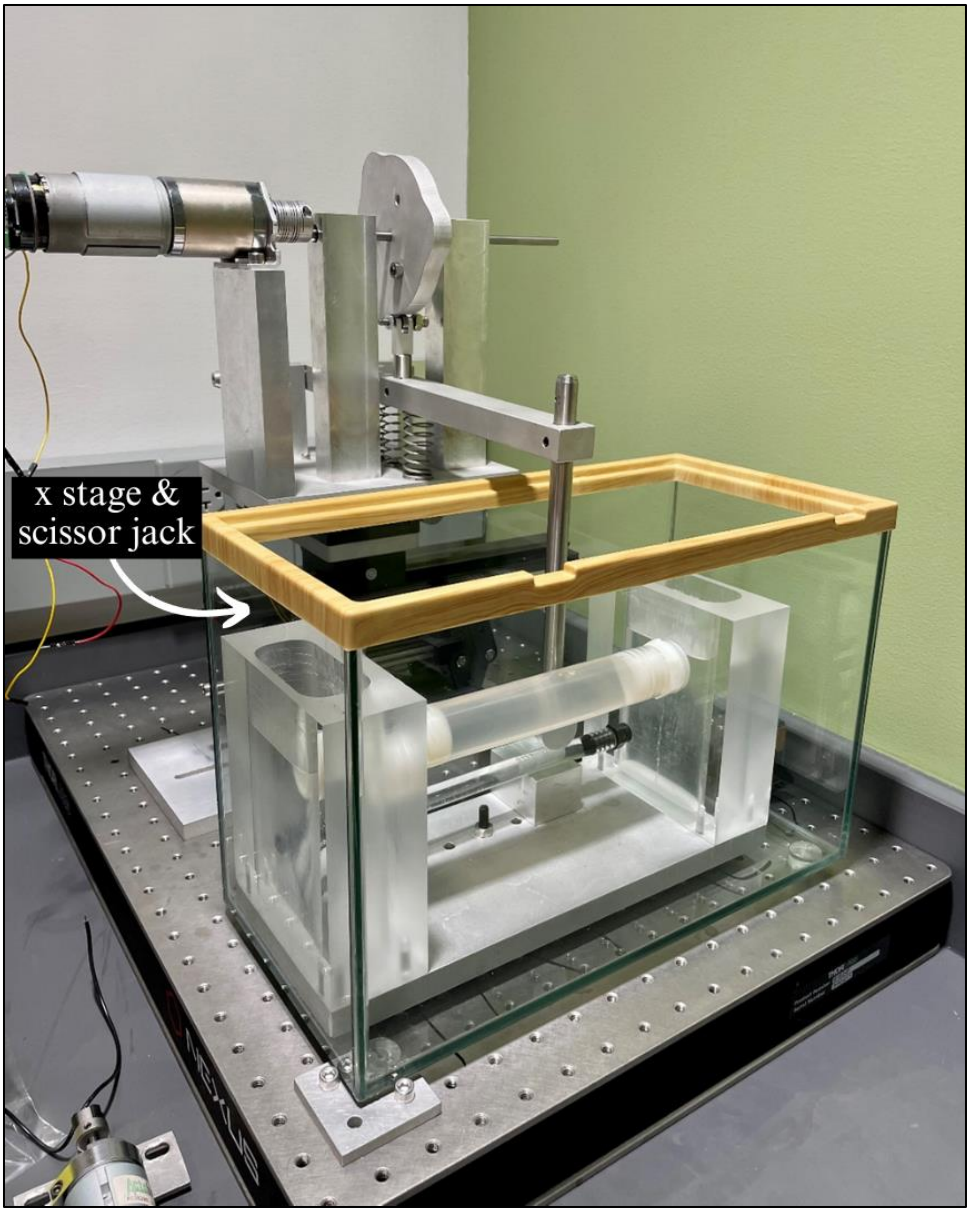

Figure 4.1. Fully manufactured system including the compression mechanism and the embryonic heart model.

4.1 Compression Mechanism Results

The assembled compression mechanism is shown in Figure 4.2 below. Several issues were discovered during testing. The first of which was that the shaft coupler, connecting the motor shaft to the cam shaft, does not stay in place. The half of the coupler that's attached to the cam shaft slides down the shaft with every rotation of

the cam. Eventually, it slides completely off, no longer interconnecting with the other half of the coupler, after about 10 revolutions. When that happens, the motor shaft is no longer connected to the cam shaft and is, therefore, no longer driving the cam shaft (the cam does not rotate).

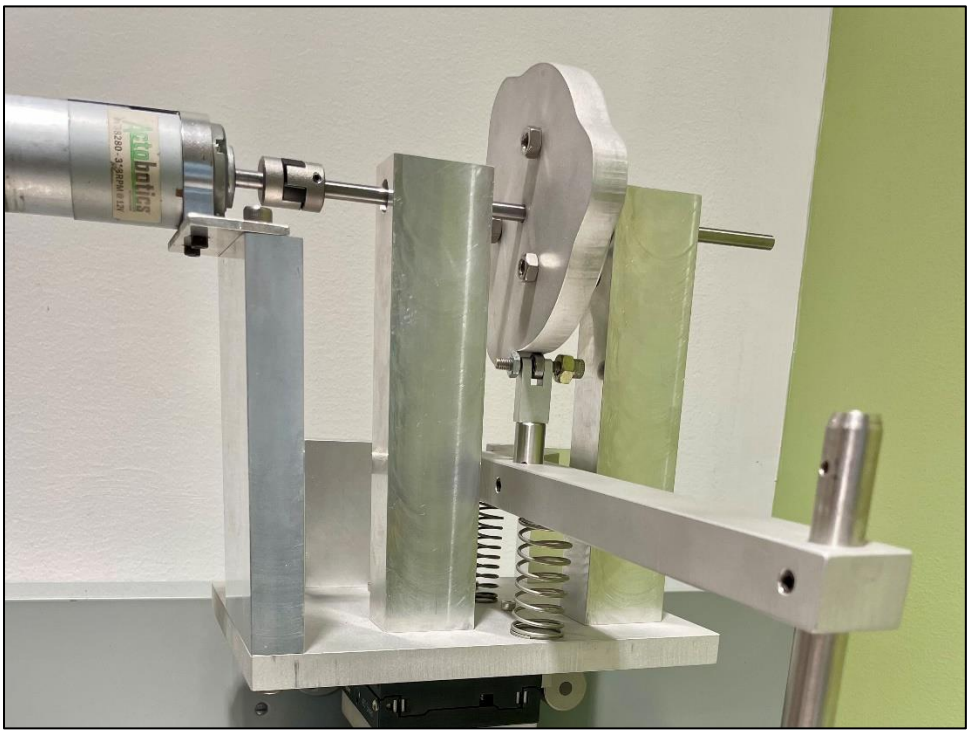

Figure 4.2. Fully manufactured compression mechanism including the cam, follower, motor, shaft coupler, and springs (extension finger and pinching attachment not shown).

The second issue with the cam mechanism is that the cam and follower slap. The follower is not properly held against the surface of the cam during the fall or spring-controlled section of each compression motion. After each rise, the follower leaves the surface of the cam and slaps back down onto it after some time in the air. See Figure 4.3 below for a visual representation of this deviation.

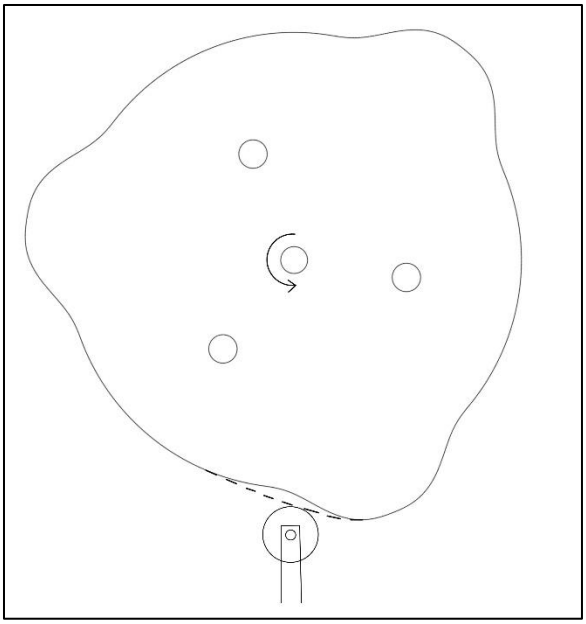

Figure 4.3. Approximate representation of the follower path with respect to the cam profile as the cam rotates counterclockwise.

This is a problem because it will cause wear on the cam and follower and because the follower is not correctly following the cam profile. That means that the position of the follower causes the arm to gradually uncompress the tube instead of more abruptly moving away, like the desired motion of cam profile.

4.2 Heart Model Results

As for the heart model, the design appears to function perfectly. The fully manufactured model is shown in Figure 4.4 below. Qualitative tests were performed, and a flow was successfully generated. For these tests, the reservoirs were filled with soapy water and the PDMS tube was compressed by hand. Soap was added to the water to create bubbles to trace the motion of the flow. In pervious designs, air bubbles within the flow could be used to track the motion. However, this open reservoir design completely removes all air bubbles from the PDMS tube.

(This was a goal of the design, because are bubbles are optical interferences in PIV testing.) For these tests, hand compressions were used in place of the cam mechanism. A Liebau pump was successfully created. Soap bubbles moving throughout the system traced the motion of a unidirectional flow.

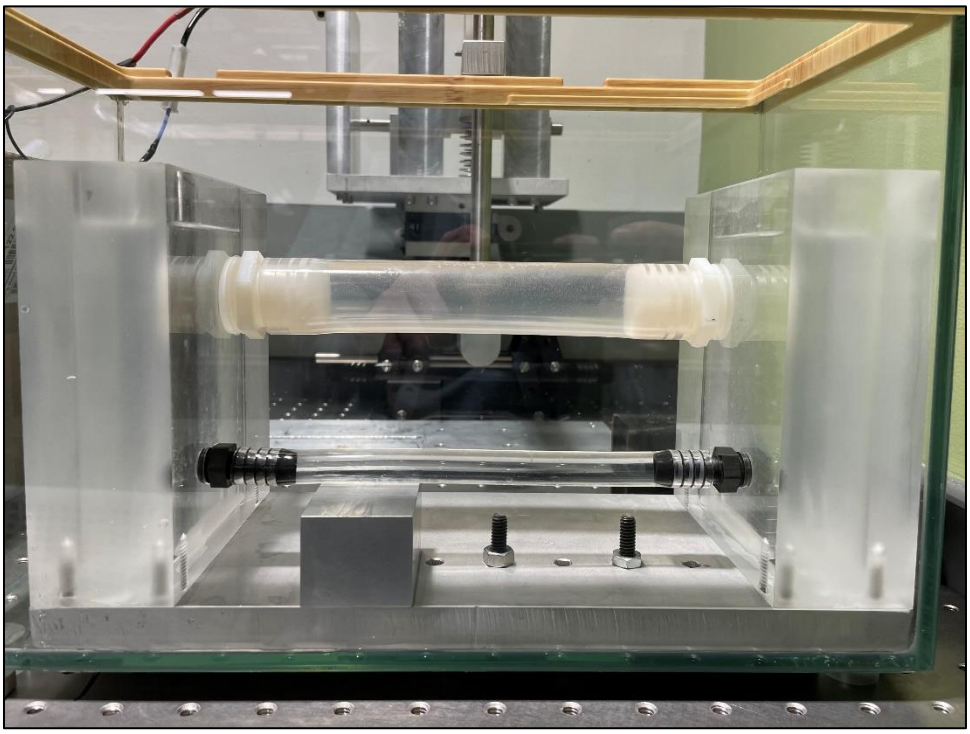

Figure 4.4. Fully manufactured heart model including the PDMS tube, connecting tube, reservoirs, and anvil.

4.3 Optical Results

Although RIM-PIV testing has not yet been performed, manufacturing the entire system has offered some further insight into the optical design. In its current state, the system only allows for RIM-PIV data to be taken just to the side of the compression point (Figure 4.5).

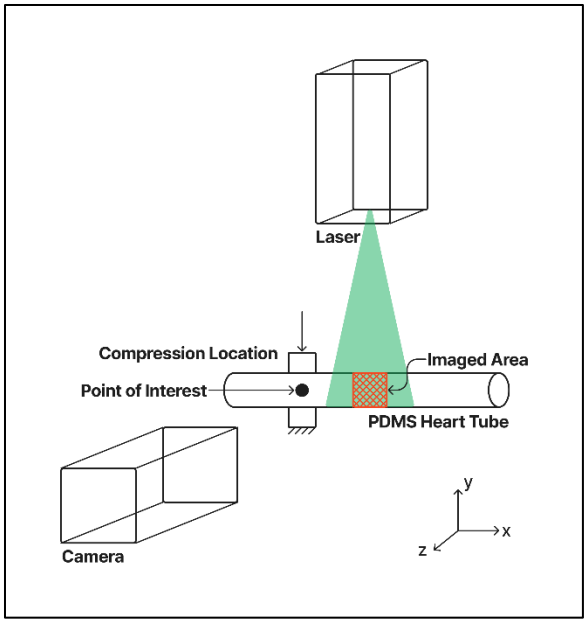

Figure 4.5. Optical layout with the imaged area to the side of the compression location/point of interest because the laser cannot shine through the pinching attachment or the anvil.

This is because the laser is obstructed by the pinching attachment from above or the anvil from below. The compression point is the location of highest interest because it is where the flow is created. Understanding what's going on there will provide the best understanding of how Liebau pumping works. With this design, whether shooting the laser from above or below, it will have to be aligned slightly to the side of the compression point, the actual location of interest.

5 Discussion

The major issues with the design appear to be with the compression mechanism. As it stands, the heart model should function as desired. Only some minor issues with the optical design were found.

5.1 Compression Mechanism Discussion

The shaft coupler problem (i.e., coupler creeping down the shaft) appears to be occurring because the torque on the motor is too much for the flexible spider between the two hubs of the coupler. When the motor rotates, the flexible spider is compressed creating a “ramp” for the cam shaft hub to slide along. Some possible ways to solve this problem are to get a stiffer shaft coupler, reduce the torque on the motor, and to lightweight the reciprocating parts. Reducing the mass will reduce the force required to accelerate the parts enough to sufficiently track the velocity changes “requested” by the cam profile.

The slapping problem appears to be occurring because the applied springs aren’t strong enough to hold the follower along the surface of the cam during the fall sections. Despite adding multiple springs under the arm, this problem persists. One possible source of this error is the length of the springs. During the spring sizing calculations, preloading was desired, so a 12.5 mm preload was added to the spring in the spring rate calculation. However, this 12.5 mm preload was forgotten in the spring length calculation. Therefore, the minimum spring length should have been 64 mm. (The spring used was 57 mm.)

A second source of error is the static system assumption used when determining the required spring force. The inertial force created when the cam accelerates the arm was wrongfully neglected. The spring should be overcoming the weight of the arm as well as that inertial force. Meaning that Equation 5.1 below would show the correct spring sizing analysis.

$$F_s = m + ma = kx \tag{5.1}$$

In this equation, F_s is the total required spring force, m is the total mass of the arm (including the arm, follower, finger, and pinching attachment), a is the arm acceleration, k is the spring rate, and x is the displacement of the spring (assumed to be 12.5 mm preloaded). The acceleration of the arm can be calculated based on the cam's angular acceleration.

All that said, using multiple springs should compensate for that problem. When more springs were used, the follower was held against the surface of the cam more forcefully. However, the spring force was too strong for the motor to overcome to compress the tube. One possible solution to this problem is to use a stronger motor and size up to the correct spring length (or continue to use multiple springs).

5.2 Optical Design Discussion

Once RIM-PIV testing begins, if it becomes a problem that the data is being taken to the side of the compression point, the overall system design could be altered to correct this issue. Because the current optical obstructions, the pinching attachment and the anvil, are vital to the function of the compression mechanism, their refractive indices will, ideally, need to be matched to the glycerin solution. If this is possible, the pinching attachment or the anvil could be made from PDMS. If they cannot be made from PDMS or a refractive index matchable material, making them from at least a transparent material would help. This "half-step" that lets the laser beam through, but is not perfectly RIM, could work and open up material choices.

This would solve the problem if these obstacles do present an issue when testing begins.

6 Conclusions & Recommendations

Overall, this Liebau pumping mechanism design should be sufficient to generate flow within the embryonic heart model. Once the changes (recommended below) are made, the entire system should function as desired. By using this device and analyzing the resulting flow (using RIM-PIV), a better understanding of Liebau pumps and their potential role in embryonic heart development should be gained.

6.1 Compression Mechanism Recommendations

Based on the problems presented in the results and analyzed in the discussion, the following actions are recommended to improve the compression mechanism design. First, the current rubber-spider shaft coupler should be replaced by a different kind of flexible shaft coupler. Now that the mechanism exists, the required motor torque, speed, and power should be determined. Then, an appropriate motor and coupler can be found.

As for the cam-and-follower slapping, this should be solved by using stronger springs (sized using the analysis described in Section 3.1.4 with the amendments describe in Section 5.1) to hold the follower along the surface of the cam, by using a motor with more torque to overcome the increased spring force, and by lightweighting the reciprocating parts (especially the steel finger). The motor mentioned in the previous paragraph is stronger than the current motor. The

motor sizing analysis describe in Section 3.1.5 should be done to confirm that this motor is sufficiently strong and fast for this application.

6.2 Heart Model Recommendations

As the heart model currently stands, there appear to be no issues. Therefore, it is recommended that the design be used as is.

6.3 Optical Layout Recommendations

Although RIM-PIV tests have not been started, the proposed optical layout and design should work for this application. As mentioned in the discussion section, it may become necessary to alter the material of the pinching attachment or the anvil. If this is case, it is recommended that the anvil be changed. Although it is safer for the user to have the laser pointing down, it might be easier to manufacture a rectangular prism from the new, RIM material than it would be to manufacture the pinching mechanism. If that is not the case, the opposite change (i.e., laser down) should be made to protect the eyesight of the user. All that said, if taking data just to the side does not present an issue, then it is recommended that the optical design remain unchanged.

7 Future Work

Beyond the modifications recommended is the previous section, the future work done on this project should include the following: Once the entire system is functional, it should be tested, and capability measurements should be taken. The

desired operating conditions (combinations of compression locations, frequencies, and amplitudes) should be chosen as desired to reach the desired conclusions on the role of Liebau pumping in embryonic hearts. Then, the entire system should be moved to Ali Hamed, Ph.D.'s PIV lab, in the Integrated Science and Engineering Complex on Union College's campus, and testing begun.

In the more distant future, the embryonic heart model should be altered to more accurately represent the embryonic heart. This can be done by scaling the model to the embryonic heart using the Buckingham Pi Theorem, mostly likely according to Reynolds number and a variable relating to compression frequency. Additionally, the geometry of the PDMS tube could be altered to reflect the changing geometries that occur as the embryonic heart develops through the looping stages. (Although, this will probably prove to be very challenging.)

Appendix

A. Bill of Materials

Table 1. Bill of purchased materials.

Item	Purpose	Vendor	Part #	Unit Price	Quantity	Total
Travel rack stage	Control position of follower arm along “heart” tube	Edmund Optics	56-793	$117.00	1	$117.00
Travel rack	Control position of follower arm along “heart” tube	Edmund Optics	56-796	$177.00	1	$177.00
Shaft coupling iron hub	Connect motor shaft to cam shaft	McMaster-Carr	6133N11	$3.76	2	$7.52
Shaft coupling rubber spider	Connect motor shaft to cam shaft	McMaster-Carr	6408K61	$3.25	2	$6.50
Qsil 2-part mix kit	Cast transparent PDMS tubes	Jensen Tools + Supply	121CH003	$69.25	2	$138.50
Glycerin	Mix a fluid to flow in and around the PDMS tube to conduct RIM-PIV	Amazon	---	$64.97	2	$129.94
Glass tank	Submerge PDMS tube in glycerin solution for RIM-PIV	Pet Smart	---	$40.00	1	$40.00
5 mm ID x 10 mm OD ball bearings	Roller follower to reduce friction on cam profile	Amazon	---	$12.99	1	$12.99

Acrylic sheet	Stock material to make reservoirs from	McMaster-Carr	8560K919	$31.92	2	$63.84
Laser pointer	Test refractive index matching of glycerin solution and PDMS tube	Amazon	---	$18.98	1	$18.98
6 mm ID x 17 mm OD ball bearings	Hold cam axel in place and reduce friction on cam axel holder	Amazon	---	$9.49	1	$9.49
Tygon tubing	Return tube that connects reservoirs	McMaster-Carr	6516T34	$10.62	1	$10.62
1" ID barbed fitting	Connects return tube to reservoirs	McMaster-Carr	5372K135	$10.86	2	$21.72
Rotary shaft	Shaft for cam to turn on because the motor shaft is too short	McMaster-Carr	1482K61	$8.60	1	$8.60
Compression spring	Hold follower against cam profile	MW Components	71722SCS	$8.91	1	$8.91
3/8" ID barbed fitting	Connects PDMS tube to reservoirs	McMaster-Carr	5218K696	$0.57	6	$3.42
1/4" long set screw	Assemble system	McMaster-Carr	91375A533	$11.41	1	$11.41
3/8" long set screw	Assemble system	McMaster-Carr	91375A535	$11.74	1	$11.74
				Grand Total		**$798.18**

B. Detailed Drawings

This appendix includes a complete detailed drawing library of all parts manufactured for this system design. The parts are ordered alphabetically by part name as shown in the table below. A complete library of SOLIDWORKS part, drawing, and assembly files can be found in the Google Drive folder linked here: https://drive.google.com/drive/folders/1f21VyvCf9poJeqCIVjsQw9fvdfPaP9H?usp=sharing.

Table 2. Manufactured parts list with name and quantity.

#	Part Name	Quantity
1	Anvil #1	1
2	Arm #3	1
3	Arm Axel Holder #1	2
4	Cam #7	1
5	Cam-Arm Plate #1	1
6	Cam-Shaft Coupler #1	1
7	Left Reservoir #1	1
8	Metric to English Conversion Plate #1	1
9	Motor Axel Holder #1	2
10	Motor Holder #2	1
11	Pincher #1	1
12	Right Reservoir #1	1
13	Roller #1 (M6 set)	1
14	Shaft Coupler #1	2
15	Tank Locator #1	2
16	Tank Plate #1	1

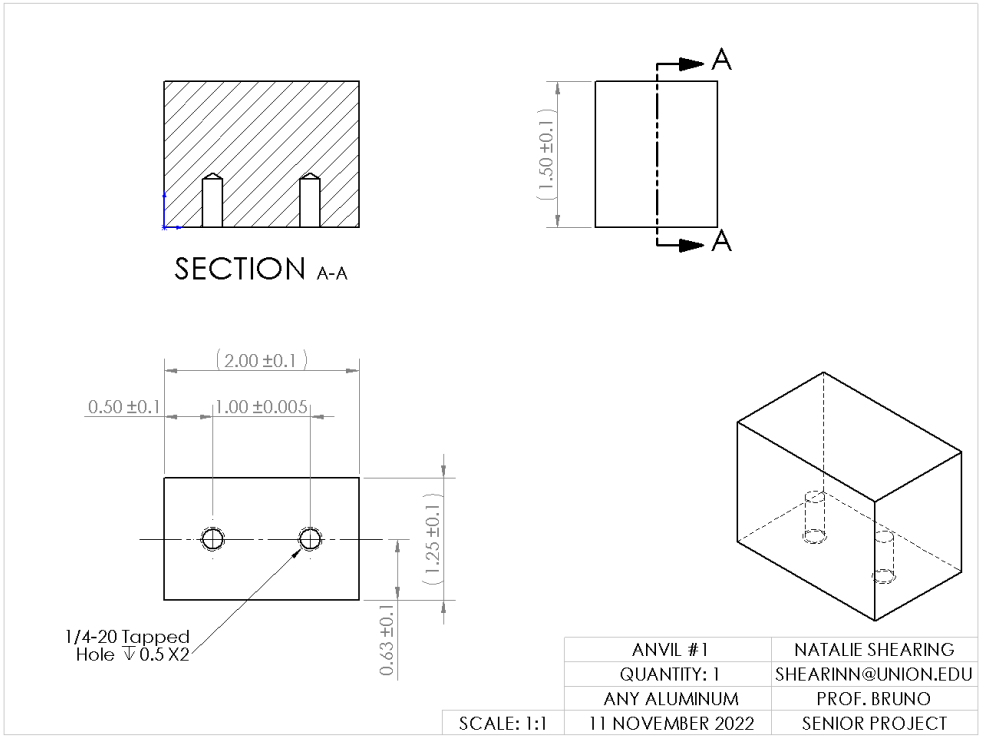

	ANVIL #1	NATALIE SHEARING
	QUANTITY: 1	SHEARINN@UNION.EDU
	ANY ALUMINUM	PROF. BRUNO
SCALE: 1:1	11 NOVEMBER 2022	SENIOR PROJECT

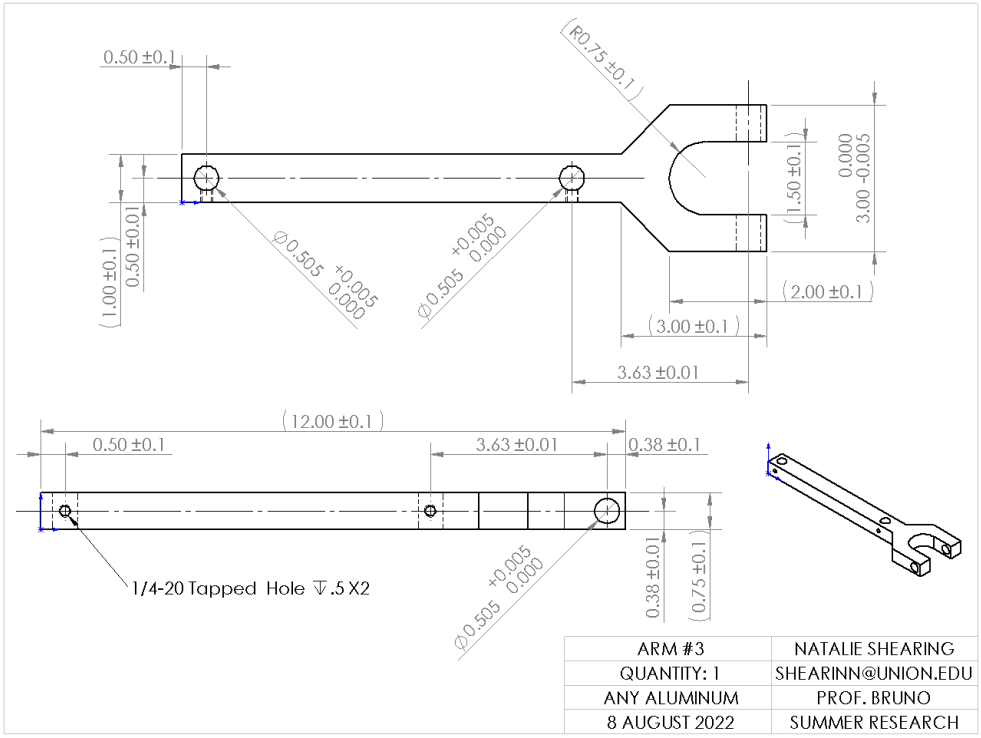

ARM #3	NATALIE SHEARING
QUANTITY: 1	SHEARINN@UNION.EDU
ANY ALUMINUM	PROF. BRUNO
8 AUGUST 2022	SUMMER RESEARCH

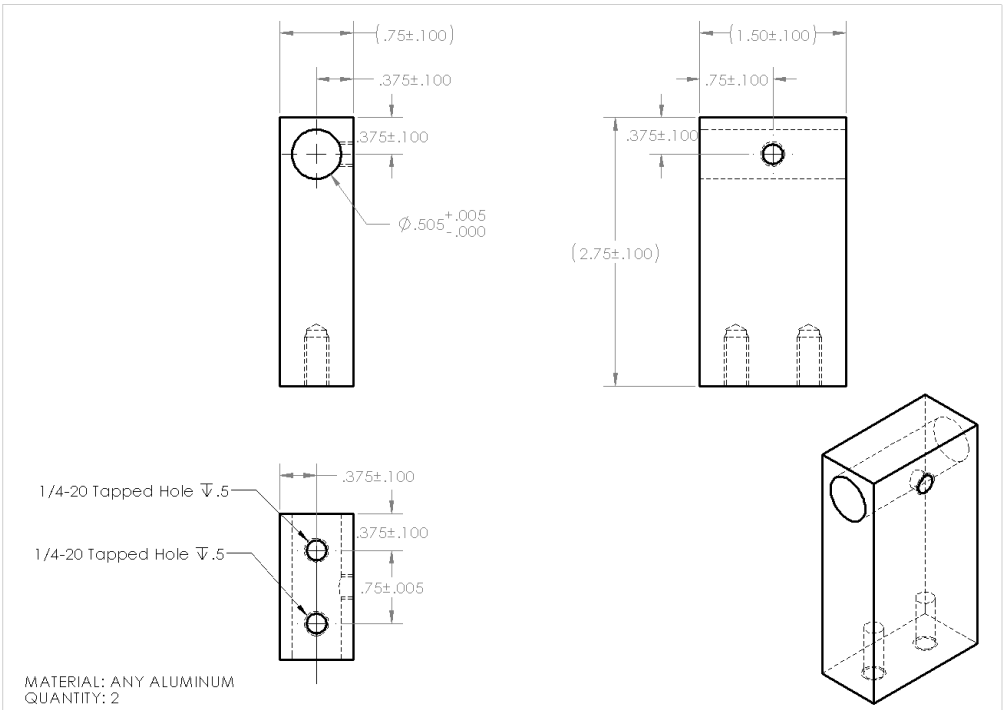

UNION COLLEGE	SUMMER 2022 RESEARCH	ARM AXLE HOLDER #1	Natalie Shearing	28 JUL 2022

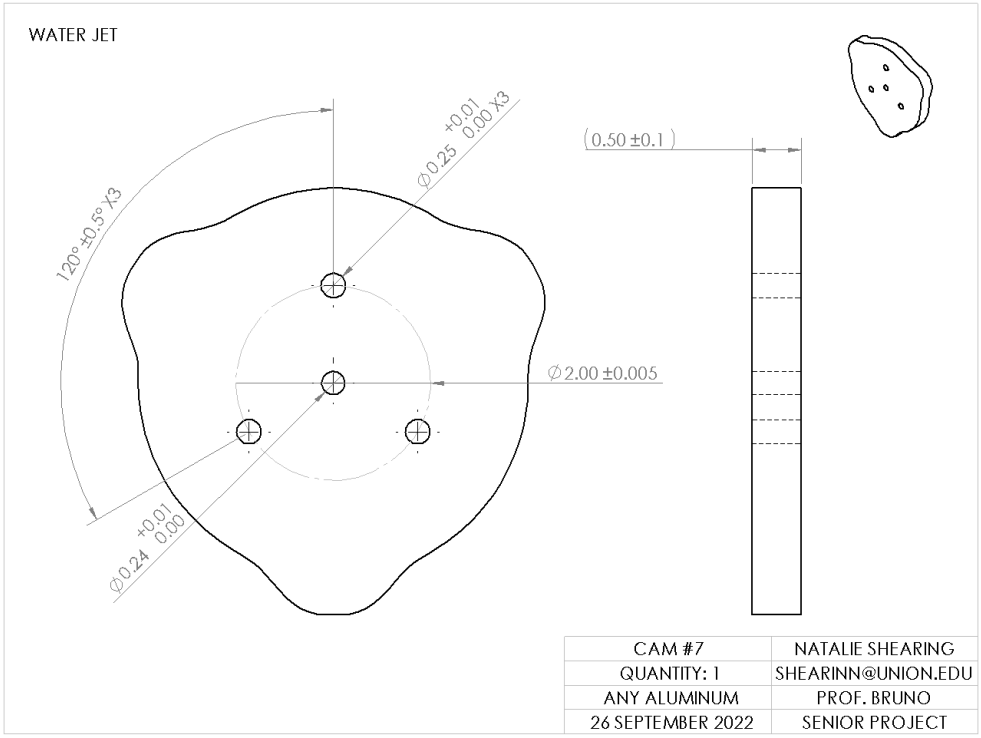

CAM #7	NATALIE SHEARING
QUANTITY: 1	SHEARINN@UNION.EDU
ANY ALUMINUM	PROF. BRUNO
26 SEPTEMBER 2022	SENIOR PROJECT

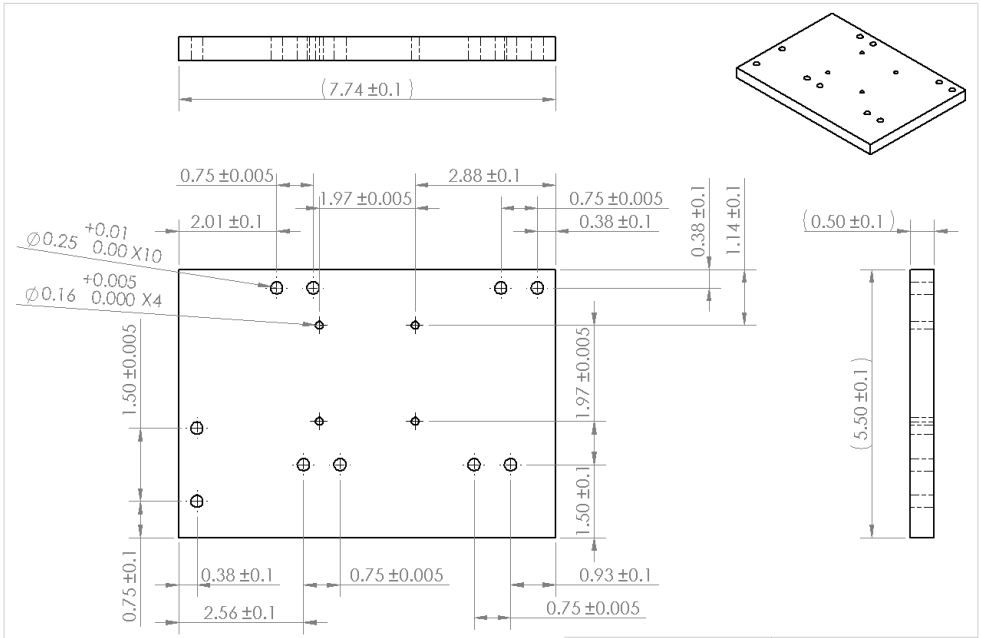

CAM-ARM PLATE #1	NATALIE SHEARING
QUANTITY: 1	SHEARINN@UNION.EDU
ANY ALUMINUM	PROF. BRUNO
26 SEPTEMBER 2022	SENIOR PROJECT

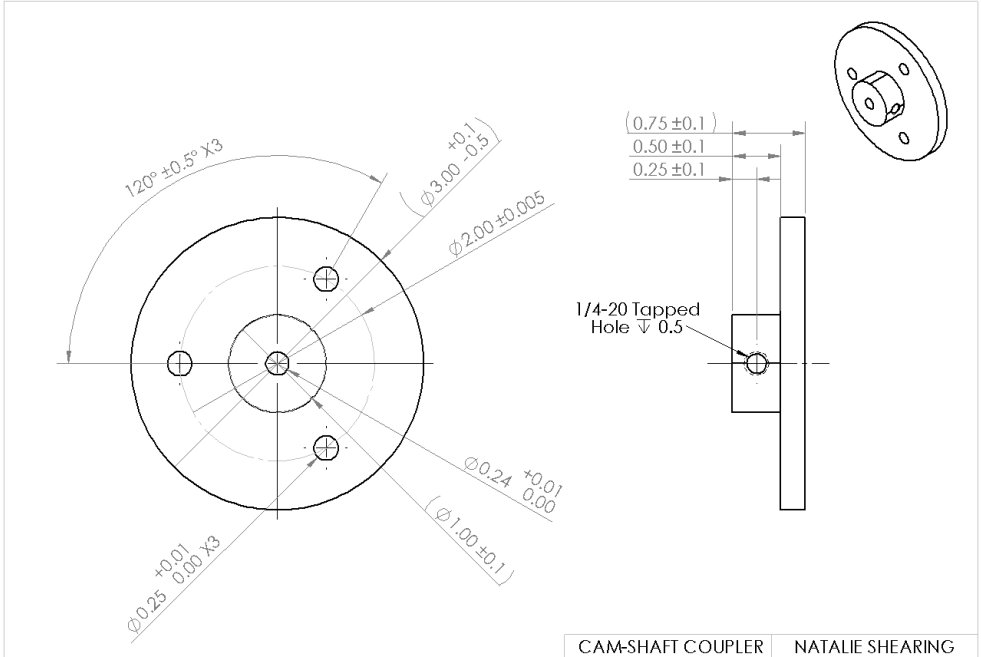

CAM-SHAFT COUPLER	NATALIE SHEARING
QUANTITY: 1	SHEARINN@UNION.EDU
ANY ALUMINUM	PROF. BRUNO
20 OCTOBER 2022	SENIOR PROJECT

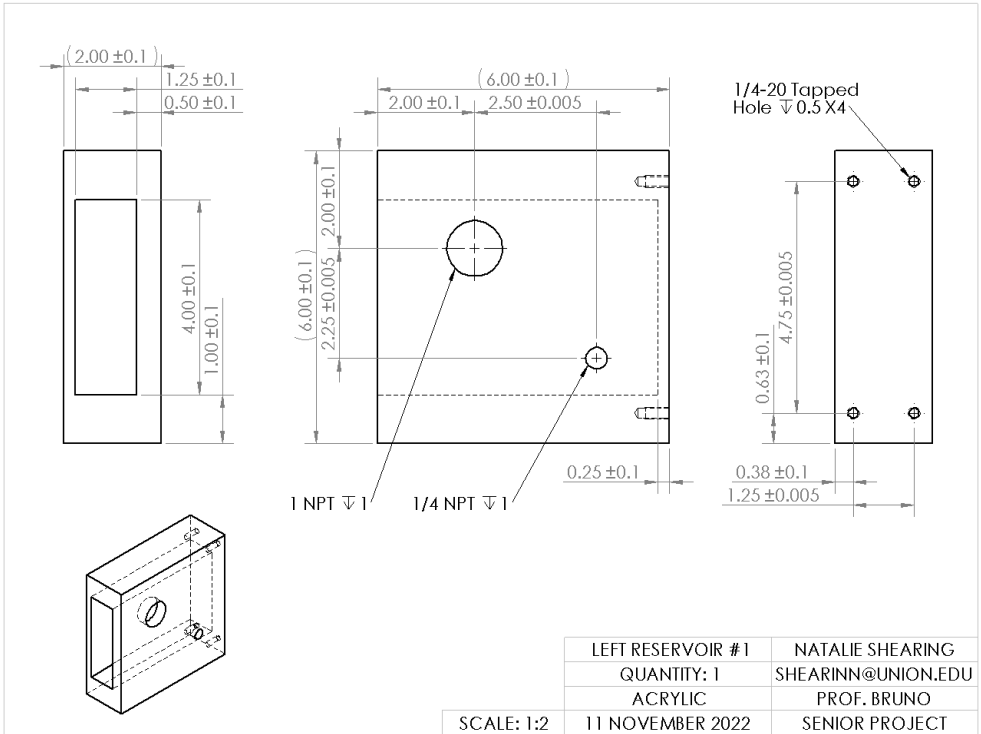

	LEFT RESERVOIR #1	NATALIE SHEARING
	QUANTITY: 1	SHEARINN@UNION.EDU
	ACRYLIC	PROF. BRUNO
SCALE: 1:2	11 NOVEMBER 2022	SENIOR PROJECT

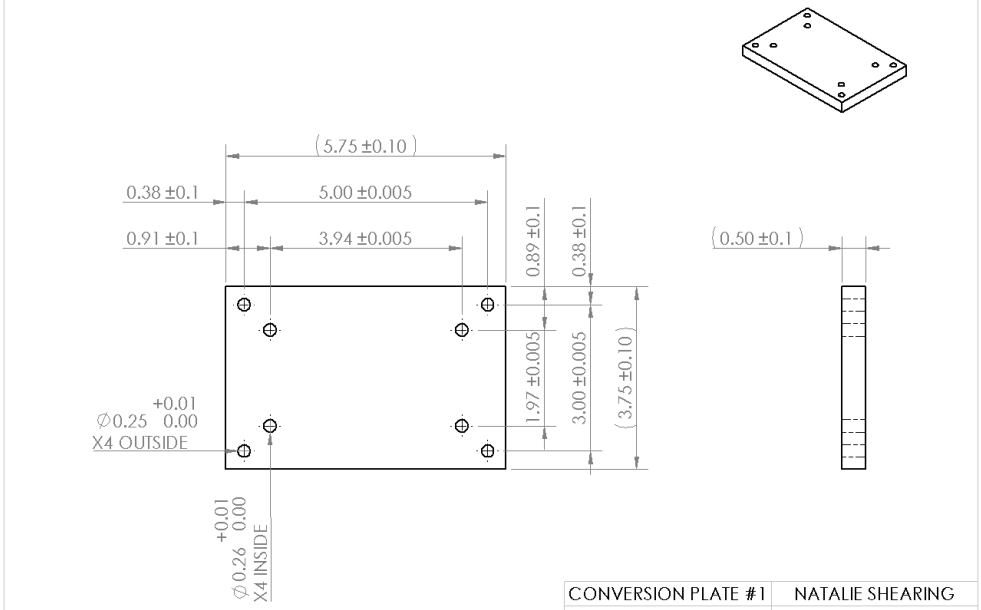

CONVERSION PLATE #1	NATALIE SHEARING
QUANTITY: 1	SHEARINN@UNION.EDU
ANY ALUMINUM	PROF. BRUNO
26 SEPTEMBER 2022	SENIOR PROJECT

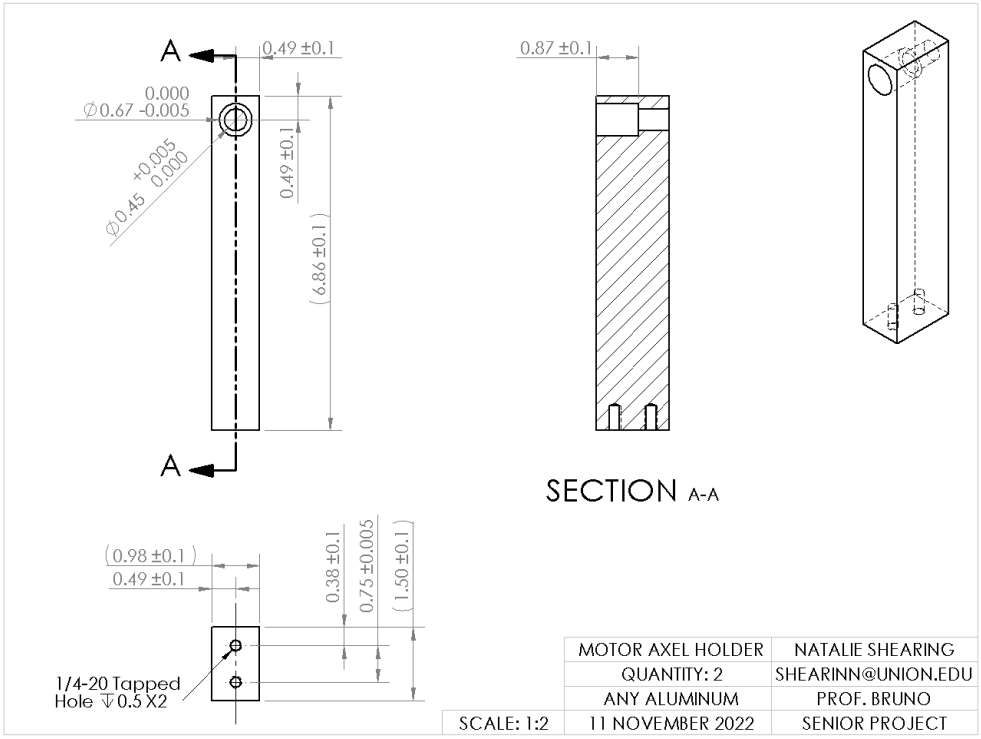

	MOTOR AXEL HOLDER	NATALIE SHEARING
	QUANTITY: 2	SHEARINN@UNION.EDU
	ANY ALUMINUM	PROF. BRUNO
SCALE: 1:2	11 NOVEMBER 2022	SENIOR PROJECT

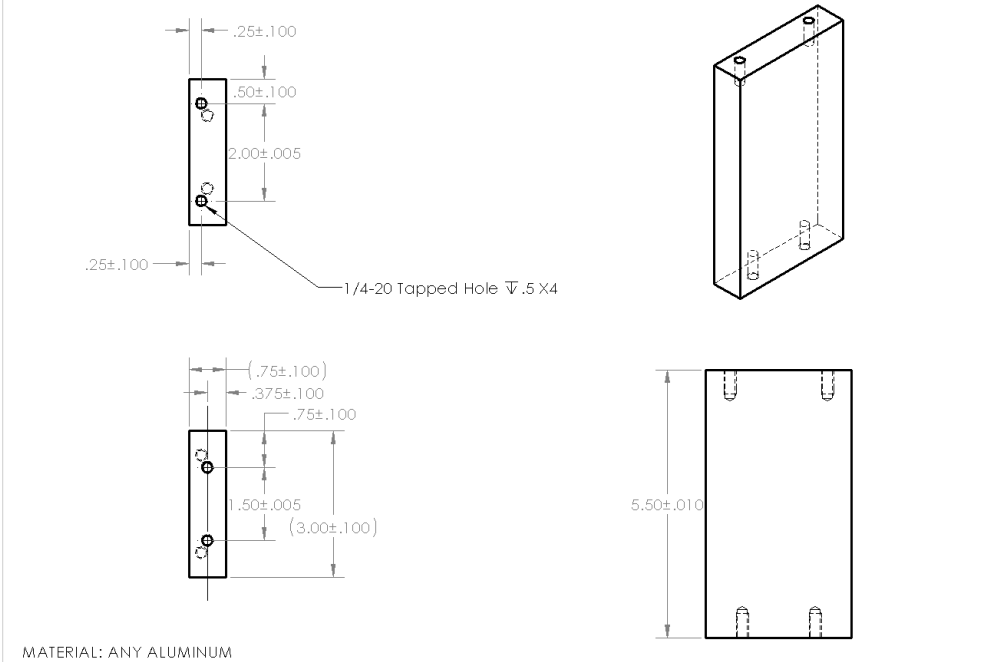

MATERIAL: ANY ALUMINUM
QUANTITY: 1

UNION COLLEGE	**SUMMER 2022 RESEARCH**	**MOTOR HOLDER #2**	**Natalie Shearing**	**29 JUL 2022**

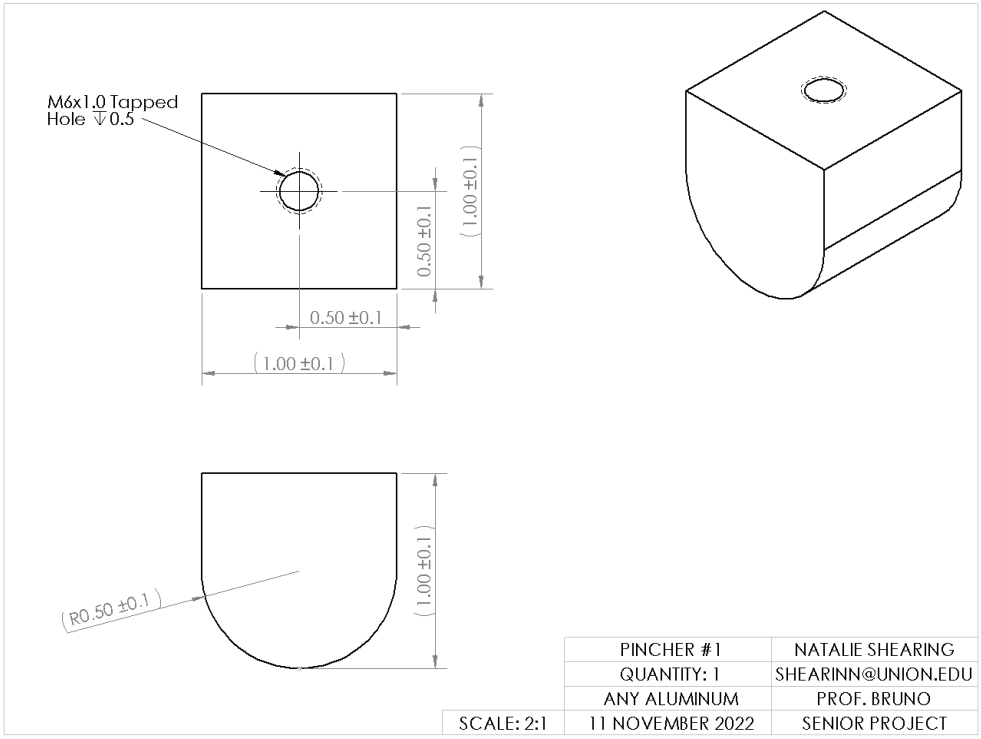

	PINCHER #1	NATALIE SHEARING
	QUANTITY: 1	SHEARINN@UNION.EDU
	ANY ALUMINUM	PROF. BRUNO
SCALE: 2:1	11 NOVEMBER 2022	SENIOR PROJECT

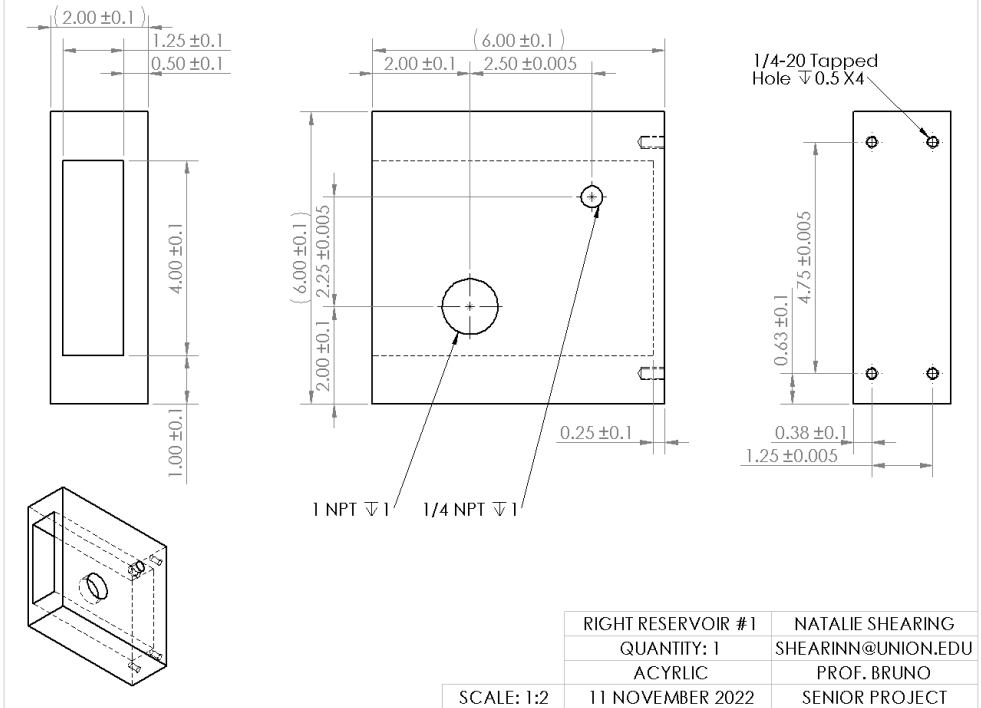

	RIGHT RESERVOIR #1	NATALIE SHEARING
	QUANTITY: 1	SHEARINN@UNION.EDU
	ACYRLIC	PROF. BRUNO
SCALE: 1:2	11 NOVEMBER 2022	SENIOR PROJECT

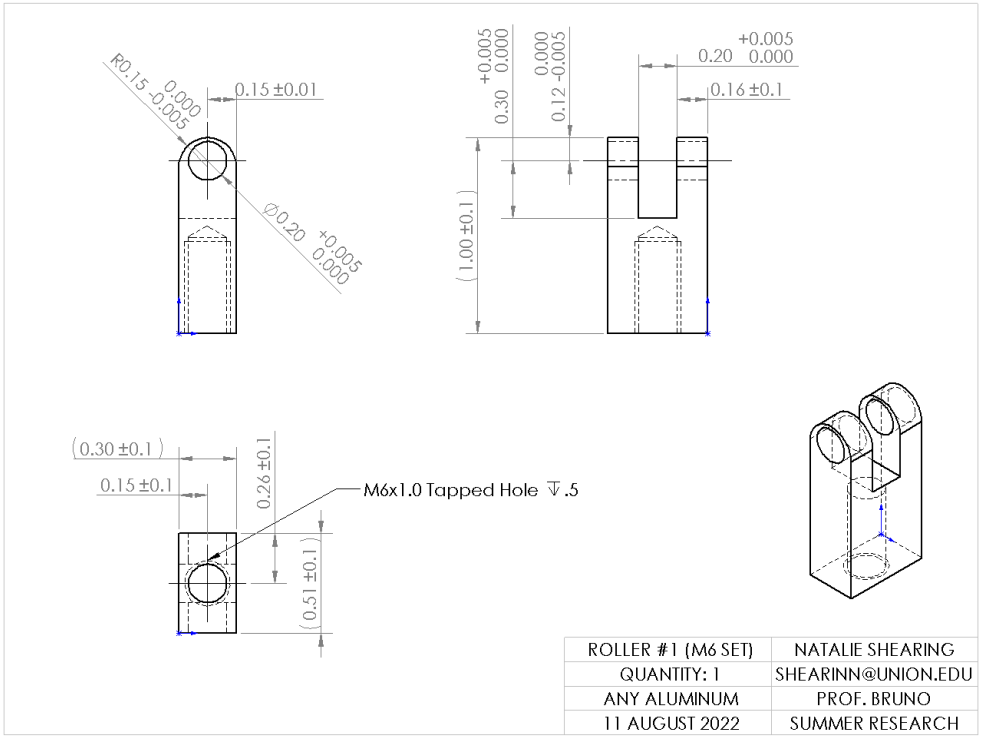

ROLLER #1 (M6 SET)	NATALIE SHEARING
QUANTITY: 1	SHEARINN@UNION.EDU
ANY ALUMINUM	PROF. BRUNO
11 AUGUST 2022	SUMMER RESEARCH

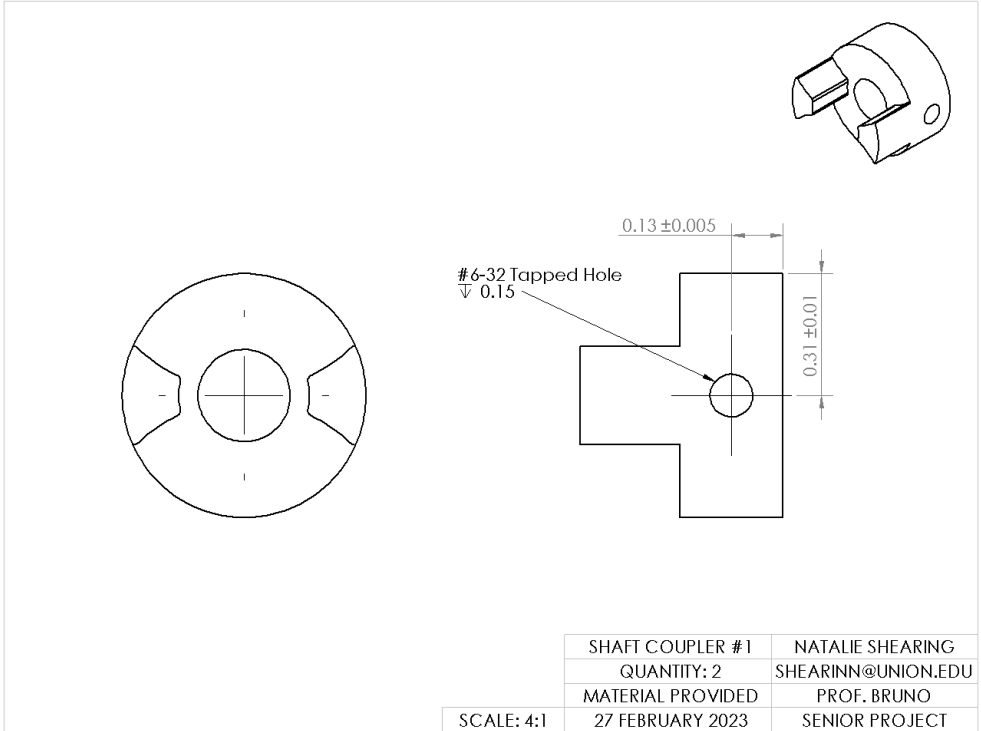

	SHAFT COUPLER #1	NATALIE SHEARING
	QUANTITY: 2	SHEARINN@UNION.EDU
	MATERIAL PROVIDED	PROF. BRUNO
SCALE: 4:1	27 FEBRUARY 2023	SENIOR PROJECT

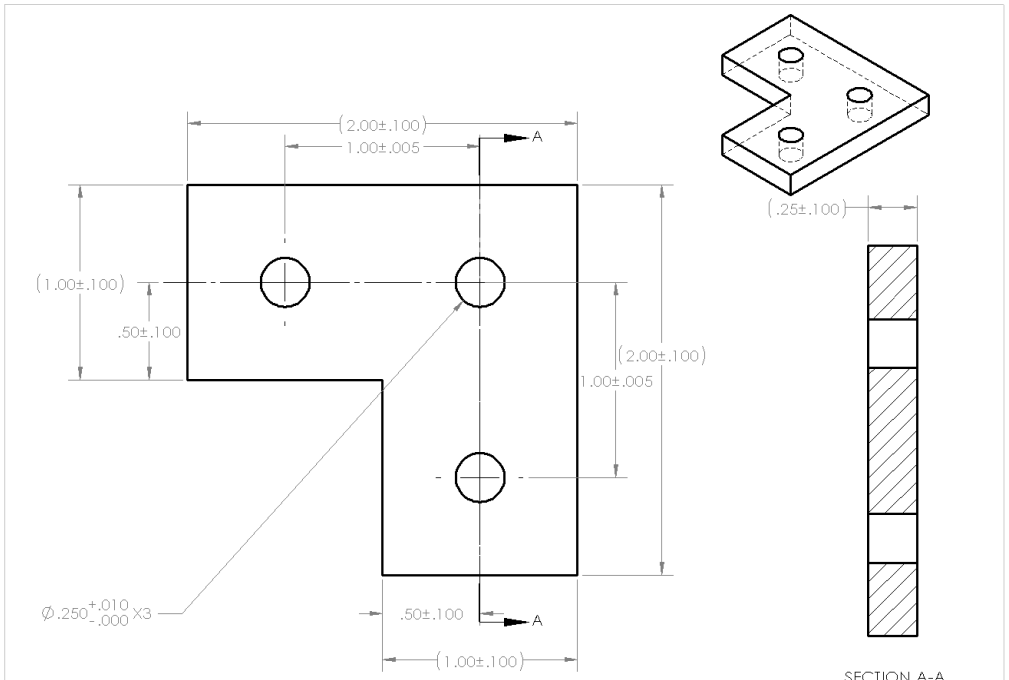

UNION COLLEGE	SUMMER 2022 RESEARCH	TANK LOCATOR #1	Natalie Shearing	29 JUL 2022

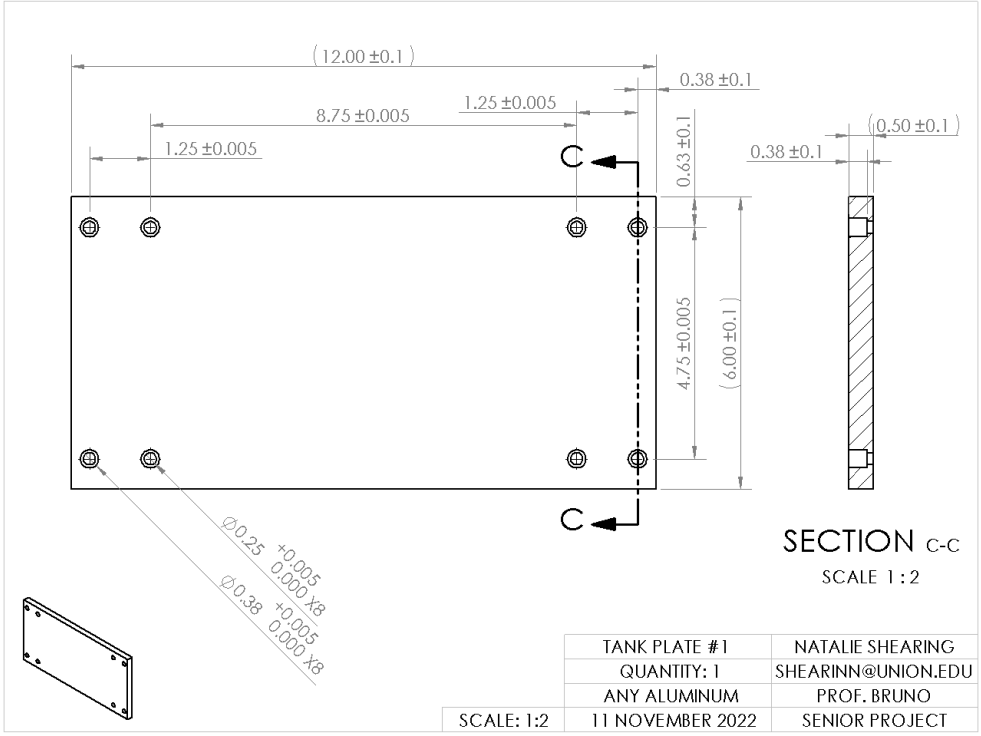

	TANK PLATE #1	NATALIE SHEARING
	QUANTITY: 1	SHEARINN@UNION.EDU
	ANY ALUMINUM	PROF. BRUNO
SCALE: 1:2	11 NOVEMBER 2022	SENIOR PROJECT

C. Previous Cam Profiles

Table 3. Previous cam profiles including maximum displacement, periods, and rejection reasoning.

Cam #	Max. Displacement, *h* [mm]	Number of Lobes	Rise & Fall Period [rad]	Dwell Period [rad]	Reason Rejected
1*	25	1	1.24	3.81	Too much torque
2*	12.5	1	π/2	π	Motor shaft hole wore out
3*	12.5	1	π/2	π	Too much torque
4	9.5	1	π	0	Too slow of rise/fall, not enough impulse, no dwell
5	12.5	4	π/6	π/6	Too slow of rise/fall, not enough impulse
6	9.5	2	π/4	π/2	Not fast enough, need higher frequency of compressions
7	9.5	3	π/6	π/3	Not rejected, used in final design

*Cams 1-3 were not designed using cycloidal functions. Their rises and falls were not smooth, and the cams often locked up, unable to turn. Also, their rise, fall, and dwell periods had to be estimated.

D. Cam Profile MATLAB Code

```
clc; close all; clear all;

% Maximum displacement
h = 0.38;

% Period of each rise, fall, and dwell
beta = 2*pi/12;

% Cam angle
t = linspace(0,2*pi,100);

% Cycloidal rise, fall, and dwell functions
for ii = 1:length(t)
   if t(ii)<beta
      s(ii) = h*(t(ii)/beta - 1/(2*pi)*sin(2*pi*t(ii)/beta));
   elseif t(ii)>=beta && t(ii)<2*beta
      s(ii) = h-h*((t(ii)-beta)/beta - 1/(2*pi)*sin(2*pi*(t(ii)-beta)/beta));
   elseif t(ii)>=2*beta && t(ii)<3*beta
      s(ii)= 0;
   elseif t(ii)>=3*beta && t(ii)<4*beta
      s(ii) = 0;
   elseif t(ii)>=4*beta && t(ii)<5*beta
      s(ii) = h*((t(ii)-4*beta)/beta - 1/(2*pi)*sin(2*pi*(t(ii)-4*beta)/beta));
   elseif t(ii)>=5*beta && t(ii)<6*beta
      s(ii)= h-h*((t(ii)-5*beta)/beta - 1/(2*pi)*sin(2*pi*(t(ii)-5*beta)/beta));
   elseif t(ii)>=6*beta && t(ii)<7*beta
      s(ii) = 0;
   elseif t(ii)>=7*beta && t(ii)<8*beta
      s(ii) = 0;
   elseif t(ii)>=8*beta && t(ii)<9*beta
      s(ii)= h*((t(ii)-8*beta)/beta - 1/(2*pi)*sin(2*pi*(t(ii)-8*beta)/beta));
   elseif t(ii)>=9*beta && t(ii)<10*beta
      s(ii) = h-h*((t(ii)-9*beta)/beta - 1/(2*pi)*sin(2*pi*(t(ii)-9*beta)/beta));
   elseif t(ii)>=10*beta && t(ii)<11*beta
      s(ii) = 0;
   else
      s(ii)= 0;
   end
end

% Plot displacement vs. cam angle
plot(t,s,'-','linewidth',2)

% Convert displacement functions into xyz and print as matrix
x = (2+s).*cos(t);
y = (2+s).*sin(t);
z =zeros(1,length(s));
A = [x' y' z']
```

References

[1] Gilboa, Suzanne, et al. “Congenital Heart Defects in the United States: Estimating the Magnitude of the Affected Population in 2010.” *Circulation* 134.2 (2016): 101-9. *MEDLINE*. Web.

[2] Courchaine, K., Rykiel, G., & Rugonyi, S. (2018). Influence of blood flow on cardiac development. Progress in Biophysics and Molecular Biology.

[3] Forouhar, A. S., Liebling, M., Hickerson, A., Nasiraei-Moghaddam, A., Tsai, H. J., Hove, J. R., Fraser, S. E., Dickinson, M. E. & Gharib, M. (2006). The embryonic vertebrate heart tube is a dynamic suction pump. *Science, 312*(5774), 751-753.

[4] Männer, J., Wessel, A., & Yelbuz, T. M. (2010). How does the tubular embryonic heart work? Looking for the physical mechanism generating unidirectional blood flow in the valveless embryonic heart tube. Developmental Dynamics, 239(4), 1035-1046.

[5] Vennemann, P., Kiger, K. T., Lindken, R., Groenendijk, B. C., Stekelenburg-de Vos, S., ten Hagen, T. L., Ursem, N. T. C., Poelmann, R. E., Westerweel, J. & Hierck, B. P. (2006). In vivo micro particle image velocimetry measurements of blood-plasma in the embryonic avian heart. *Journal of Biomechanics*, 39(7), 1191-1200.

[6] Kozlovsky, P., Bryson-Richardson, R. J., Jaffa, A. J., Rosenfeld, M., & Elad, D. (2016). The driving mechanism for unidirectional blood flow in the tubular embryonic heart. *Annals of Biomedical Engineering, 44*(10), 3069 3083.

[7] Männer, J. (2000). Cardiac Looping in the Chick Embryo: A Morphological Review With Special Reference to Terminological and Biomechanical Aspects of the Looping Process. *The Anatomical Record*, 259, 248-262.

[8] Hamed, Ali M., et al. Proposal to the National Science Foundation for Major Research Instrumentation: High-speed, volumetric, three-component particle image velocimetry system. 21 Jan. 2019.

[9] Nadire, Liam and Bradford Bruno. "Liebau Pumping: A RIM-PIV Study of Valveless Pumping." Union College, Mar. 2019.

[10] Hickerson, Anna. "An Experimental Analysis of the Characteristic Behaviors of an Impedance Pump." Ph.D. Thesis. California Institute of Technology, Apr. 2005.